EXTRACELLULAR CALCIUM ION DEPLETION IN FROG CARDIAC VENTRICULAR MUSCLE

KARL P. DRESDNER AND RICHARD P. KLINE
Departments of Pharmacology and Medicine, Mount Sinai Medical Center, City University of New York, New York, New York 10029

ABSTRACT The extracellular free [Ca^{++}] in frog ventricular muscle strips was monitored using single-barrel calcium ion-selective microelectrodes. During trains of repetitive stimulation, a heart rate-dependent, sustained fall (depletion) of the extracellular free [Ca^{++}] occurs, which is most likely a consequence of net Ca^{++} influx into ventricular cells. The magnitude of the $[Ca^{++}]_o$ depletion increases for higher Ringer's solution [Ca^{++}], and is reversibly blocked by manganese ion. Prolonged repetitive field stimulation (20–30 min) activates additional cellular Ca^{++} efflux, which can balance the additional Ca^{++} influx caused by stimulation, resulting in abolition of extratrabecular $[Ca^{++}]_o$ depletion in 20–30 min, and hence zero net transmembrane Ca^{++} flux at steady state. In the poststimulation period of quiescence, cellular Ca^{++} efflux persists and causes an elevation (accumulation) of the extracellular free [Ca^{++}]. From these $[Ca^{++}]_o$ depletions, quantitative estimates for the net transmembrane Ca^{++} flux were derived using an analytical solution to the diffusion equation. In the highest Ringer's solution [Ca^{++}] used (1 mM) the calculated net increase of the total intracellular calcium per beat was 6.5 ± 1.4 μmol/l of intracellular space. This corresponds to an average net transmembrane Ca^{++} influx of 0.81 ± 0.17 pmol/cm^2/s during the 800-ms action potential. In lower bath [Ca^{++}] the net transmembrane [Ca^{++}] flux was proportionately reduced.

INTRODUCTION

The cardiac cell membrane potential activates a transmembrane movement of calcium ions that may serve to directly activate the contractile proteins (Chapman, 1979), trigger calcium release from the sarcoplasmic reticulum (Fabiato and Fabiato, 1978), or replenish this store. Proposed pathways for this Ca^{++} influx, activated by membrane depolarization, include calcium ion channels (Rougier et al., 1969) and Na^+/Ca^{++} exchange (Mullins, 1977). Intracellular calcium ion-selective microelectrodes (Lee et al., 1980) and intracellular aequorin, a calcium-sensitive photoprotein (Allen and Blinks, 1978), have been used to study changes in the cytoplasmic calcium ion concentration. However, these measurements cannot indicate whether the cytoplasmic [Ca^{++}] fluctuation is due to release of Ca^{++} from an intracellular organelle or due to entry from the extracellular fluid. However, extracellular calcium microelectrodes can specifically measure extracellular calcium changes due to Ca^{++} leaving the extracellular fluid.

There are several possible reasons for finding $[Ca^{++}]_o$ fluctuations in the frog heart: (*a*) narrow and tortuous extracellular spaces occur between frog ventricular cells and trabecula (Page and Niedergerke, 1972), thus delaying the equilibrium of the extracellular calcium concentration during beating (Attwell et al., 1979); (*b*) the ratio of the cardiac cell membrane surface area to extracellular cleft volume is large (Cohen and Kline, 1982); and (*c*) the long duration of the frog ventricular action potential (600–1,000 ms) causes integration of the effects of the net Ca^{++} flux (Cohen and Kline, 1982).

Here we report that frog ventricular muscle transmembrane Ca^{++} fluxes can be continuously studied when an extracellular calcium ion-selective microelectrode is used to measure changes in the $[Ca^{++}]_o$ accompanying repetitive membrane excitation. Preliminary data have appeared in abstract form at the 1982 and 1983 Biophysical Meetings (Dresdner et al., 1982; Dresdner and Kline, 1983). Since we first reported our finding of extracellular calcium depletion in cardiac tissue, several investigators have confirmed our basic findings in frog ventricle (Hilgemann and Langer, 1984*a*; Cleeman and Morad, 1984) and in mammalian tissue (Hilgemann et al., 1983; Hilgemann and Langer, 1984*b*) using optical techniques, and also calcium-sensitive microelectrodes (Bers, 1983).

METHODS

Strips (~1 mm in cross section and 3–4 mm long) of frog (*Rana pipiens*) midventricular myocardium were held on the bottom of a Plexiglas tissue bath by a mesh of surgical threads or with two fine insect pins and

Address all correspondence to Richard P. Kline, Pharmacology Department, College of Physicians and Surgeons, Columbia University, 630 West 168th Street, New York, New York 10032.

The present address for both Dr. Dresdner and Dr. Kline is the Pharmacology Department, College of Physicians and Surgeons, Columbia University, 630 West 168th Street, New York, New York 10032.

superfused with a Ringer's solution (22°C) containing (in millimoles per liter): 3 KCl, 92.5 NaCl, 25 $NaHCO_3$, 0.5 NaH_2PO_4, 0.02 $MgCl_2$, 0.05–1.0 $CaCl_2$, 5.5 glucose, and gassed with 95% O_2/5% CO_2 to yield a pH of 7.25 ± 0.05. For at least 2 h before the experiment, the tissue was field stimulated with 2–6 ms, 2–6 mA current square pulses at a constant rate of 3–12 per minute using two Ag-AgCl wires that were attached to a stimulus isolator (Bloom Associates, Narbeth, PA).

The bath, preamplifiers, and microelectrodes were enclosed inside a copper-screen Faraday cage. The bath was grounded via a 2 M KCl/2% agar bridge, one end of which was lowered into a 2 M KCl reservoir. A Ag-AgCl electrode, connected to ground, was inserted into the reservoir. The ion-selective electrodes were connected to high impedance multiple-channel differential amplifiers (Bloom Associates; Metametrics Inc., Cambridge, MA); which had input impedances of 10^{14} Ω. A 10^{11}-Ω input impedance, 100 kHz frequency-response electrometer (M-707; W-P Instruments, Inc., New Haven, CT) was used to measure transmembrane potentials recorded by 8–20 MΩ resistance glass microelectrodes filled with 3 M KCl.

Single-barrel Ca^{++} ion-selective microelectrodes (Ca-ISEs) were made by placing a small amount of neutral Ca^{++} carrier cocktail (Oehme et al., 1976; Fluka Chemical Co., Hauppauge, NY) in the tips of silanized aluminosilicate glass micropipettes (Glass Co. of America, Bargintown, NJ). The aluminosilicate glass is harder and has about two orders of magnitude higher electrical resistance then the borosilicate No. 7740 glass. This glass (2 mm outer diameter, 14% wall thickness) required a stronger electrode puller and we used a vertical puller (model PE-2; Narashige Scientific, Tokyo, Japan) for this purpose. After the pull, the tips were slightly broken under microscopic observation to 1.5 to 2.5 μm outer diameter by touching the tip to the flattened face of a silver wire using a micromanipulator.

The micropipettes were silanized after drying for 1 h at 110 ± 10°C, while laying flat in a covered Pyrex Petri dish. They were then exposed to trimethylchlorosilane gas (boiling point 56°C) by our placing several drops of the trimethylchlorosilane liquid through a small hole in the lid of the Petri dish. The hole in the lid was then covered for several hours at which time the dish was vented. The micropipettes were then cooled and backfilled with a degassed 100 mM $CaCl_2$ solution. Using suction applied to the open end of the micropipette, a column (500 to 1,500 μm in length) of calcium-sensitive resin (Oehme et al., 1976) was pulled into the tip.

Ca-ISEs were calibrated at 22°C before and after each experiment (see Fig. 1). The calibration solution composition (in millimoles per liter) was: 3 KCl, 118 NaCl, 0.02 $MgCl_2$, with 0.005, 0.010, 0.050, 0.10, 0.20, or 1.0 $CaCl_2$. The 5 μM $[Ca^{++}]$ solution was buffered with HEDTA (Martell and Smith; 1974) and buffered at pH 7.03 with imidazole in the absence of Mg^{++}. Following the note of Tsien and Rink (1980) the single proton association constants of HEDTA were increased by 0.11 log units in 0.1 M ionic strength solutions (Martell and Smith, 1974). The calculated apparent association constant of HEDTA for Ca^{++} at pH 7.03 was $10^{5.301}$. The Ca-ISEs that were used in the physiological experiments had a Nernstian slope of 29 ± 3 mV (n = 45). Occasionally a Ca-ISE had a super-Nernstian slope (45 to 55 mV) between 10^{-6} and 10^{-4} M $[Ca^{++}]$ (see Lee, 1981; Dagostino and Lee, 1982), but these electrodes were not used.

To compare the electrodes we constructed with those reported by other authors, we also performed a series of calibration experiments at much lower calcium levels, well below those encountered in the extracellular space. Thus we calibrated some of the Ca-ISEs in 10^{-8}, 10^{-7}, and 10^{-6} M free $[Ca^{++}]$. The results of such additional calibration studies are also shown in Fig. 1 (see caption for details). They indicate that the Ca-ISEs used in this study compare favorably with those generally used for intracellular measurements.

We have examined possible errors due to extracellular fluid Na^+ and K^+ interference during our experiments. In our experiments using 0.050 mM $[Ca^{++}]$ Ringers's solution, the extracellular $[Ca^{++}]$ may fall during repetitive trains of action potentials, to 0.010 mM in the center of a muscle strip. This represents the maximum depletion of $[Ca^{++}]_o$ observed in the lowest bath calcium Ringer's solution used. During this extracellular $[Ca^{++}]$ depletion, the largest expected extracellular potassium ion concentration increase is 10 mM (Kline and Morad, 1978). We assume that the extracellular $[Na^+]$ falls by a similar amount (10 mM).

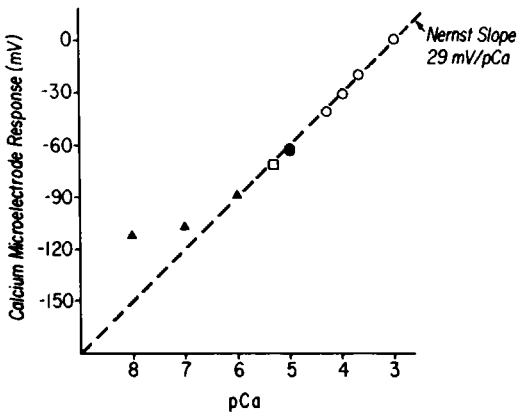

FIGURE 1 The figure shows a calibration graph of Ca-ISE response (in millivolts) as a function of the pCa (negative log of the free calcium ion concentration). The pCa 3 to 5.3 solutions (1.0 to .005 mM $[Ca^{++}]$) have a constant ionic strength of 0.12 M (data plotted with O with the exception of pCa 5.3, which is nitriloacetic acid buffered [see text] and denoted by □). The solid circle (●) is pCa 5 response with K^+ = 20 mM/Na^+ = 101 mM vs. open circle (O) at pCa 5 where K^+ = 3 mM/Na^+ = 118 mM. These two pCa 5 responses vary by <1 mV (note overlap of symbols) and indicate that worst case extracellular K^+ and Na^+ fluctuations will not cause significant error during measurement of extracellular Ca^{++} depletion. The dashed line has a slope of −29 mV per pCa unit in the range of 0.005 to 1.0 mM $[Ca^{++}]$ indicating that $[Ca^{++}]$ can be simply calculated by treating the Ca-ISE response as logarithmic function of $[Ca^{++}]$. Open circle points are the means of observations with 45 Ca-ISEs. The solid triangles (▲) are Ca-ISE responses to pCa 6,7,8 solutions. These solutions were EGTA buffered and pH buffered to 7.0 using imidazole. They contained (in millimoles per liter): 140 KCl, 6 NaCl, and 1 $MgCl_2$ as per Lee et al. (1980). However, the correction noted by Tsien and Rink (1980) was applied. Namely, the single proton association constants of EGTA in 0.15 molar ionic strength were increased by 0.12 log units (Martell and Smith, 1974). The calculated apparent association constant of EGTA for Ca^{++} at pH 7.00 was $10^{6.41}$. The pCa 6,7, and 8 responses of the Ca-ISEs confirm observations of other investigators (Lee et al., 1980; Tsien and Rink, 1980; Dagostino and Lee, 1982) with regard to the limit of detection of calcium.

Using the Nicolsky equation and values for the selectivity coefficients for Na^+ and K^+ interference (k_{CaNa} = 5 × 10^{-5}, k_{CaK} = 5 × 10^{-6}; Dagostino and Lee, 1982) the background ion interference was estimated in extracellular Ringer's solutions containing (in millimoles per liter) 118 Na^+/3 K^+ and in 108 Na^+/13 K^+. The Ringer's solution containing 118 Na^+, 3 K^+, and 0.010 Ca^{++} would appear to the Ca-ISE to contain 11.2 μM free $[Ca^{++}]$, whereas the extracellular Ringer's solution with 108 Na^+, 13 K^+, and 0.010 Ca^{++} would appear to contain 11.0 μM free $[Ca^{++}]$. This calculation was confirmed with special calibrating solutions in which K^+ was substituted for Na^+. Thus the error in measuring the magnitude of $[Ca^{++}]_o$ depletion, with extracellular $[Na^+]$ simultaneously depleting and extracellular $[K^+]$ accumulating, was about a 2% overestimate when we consider this worst case example. The results of this test of the effects of changes in background ions are also plotted in Fig. 1.

During quiescence, the 50 μM $[Ca^{++}]_o$ for a lowest calcium Ringer's solution would appear to be ~51 μM, due to the interference of the background Na^+ for the least selective Ca-ISEs measured (see above). This was an additional source of error, about a 2% underestimate in measuring the $[Ca^{++}]_o$ depletion.

The electrical noise of these high impedance Ca-ISEs was observed to be between 0.2 and 0.4 mV (peak-to-peak). An uncertainty of 0.5 mV

corresponded to a 4% uncertainty in measuring steady Ca^{++} levels. This uncertainty due to electrical noise was constant, whereas the errors due to interfering ions were reduced when higher bath calcium Ringer's solution was used.

The calcium ion activity coefficient in our 0.12 M ionic strength Ringer's solution is estimated to be 0.34. (This is based upon interpolation of values of 0.35 and 0.32 reported by Lee [1981] for 0.10 and 0.15 M ionic strength Ringer's solutions.) Although the Ca-ISE actually measures the calcium ion activity, we have assumed that the calcium ion activity coefficient of the Ringer's solution in the bath and in the extracellular spaces are the same. Thus, when reporting physiological results, we have referred to all CaISE outputs as the extracellular calcium ion concentration standardized against the known Ringer's solution calcium ion concentration.

The chemical (by rapid bath changes; see Fig. 2 *a*) and the electrical (ramp pulse method, Kline and Morad, 1978; see Fig. 2 *b*) time constants of the Ca-ISEs constructed for extracellular use were similar and averaged <1 s. The rate of response of these Ca-ISEs was adequate to follow the extratrabecular space $[Ca^{++}]_o$ depletions and accumulations in frog ventricle, which had much slower time constants (20–120 s). Baseline drift of the Ca-ISEs employed in the experiments reported here ranged from +0.6 to +3.0 mV/h. These Ca-ISEs had a useful lifetime of 3–10 h.

The relatively fast response time of the electrodes and the slow stimulus rates used for many of these experiments meant that polarization of the

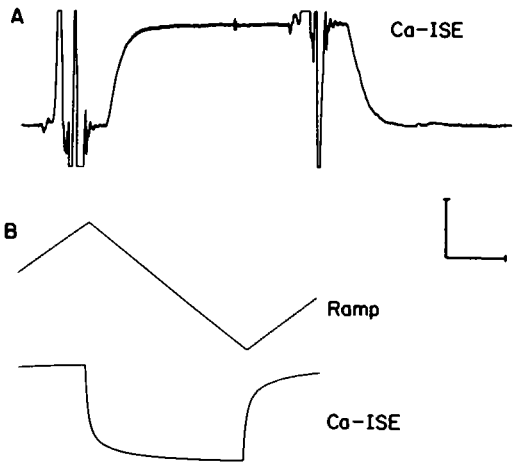

FIGURE 2 The *top* trace (*A*) shows the response of the Ca-ISE to a rapid doubling of the calcium concentration of the bath Ringer's solution (0.1 to 0.2 mM) by means of a rapid perfusion, small volume bath. The bath change was complete in 0.5 s as determined with a K-ISE (data not shown), whose response time was more than ten times faster than the Ca-ISE. Ca-ISE response time constant was 1 s (horizontal calibration bar indicates 4 s). The magnitude of the Ca-ISE response was 10 mV (vertical calibration bar indicates 5.7 mV). The solution was returned to the lower calcium value after 16 s. Artifacts preceding the changes in bath calcium are caused by the solution valve. The signal-to-noise ratio here is 25. The *bottom* two traces (*B*) show a triangular ramp pulse (*top*), which is coupled to the input of the Ca-ISE amplifier through a 1-pF capacitor. The Ca-ISE response is shown as the *bottom* trace. This method (see Kline and Morad, 1978) is used to independently assess the electrical time constant of the Ca-ISE. It is preferable to changing the bath potential with a square pulse since the capacitive coupling between the bath electrolyte solution and the Ca-ISE walls generate an artifactually low estimate of the electrode electrical response time. The vertical calibration bar indicates 40 mV for the ramp pulse and 4 mV for the electrode response. The horizontal calibration bar indicates 4 s. The Ca-ISE response to the ramp pulse (10.8 s in duration) is 95% complete within 3.7 s. The response could not be reduced to either one or two exponentials.

Ca-ISE response due to stimulus artifacts was not a problem. In fact the stimulus artifact was generally seen as a discreet response that returned to baseline before the full development of the small calcium depletions seen during single beats. As a routine precaution, we exposed the Ca-ISE (tip in the bath) to rapid stimulus trains of intensity and duration several times normal values. We failed to see any summation of the rapid stimulus artifact spikes. During physiological measurements (tip in the muscle extracellular space), the presence of the slow negative going Ca-ISE response (indicative of calcium depletion) was an all or nothing response that occurred at the same stimulus threshold as that for excitation of the membrane and generation of an action potential. The stimulus artifact varied in a graded fashion with stimulus intensity, and reversed polarity for reversal of stimulus polarity. The Ca-ISE response in the muscle was invariant to stimulus polarity for threshold stimulus trains.

To permit stable and prolonged extracellular calcium measurements, twitch tension was reduced by lowering the bath Ringer's solution $[Ca^{++}]$ as had been done by Kline and Morad (1976, 1978) and Martin and Morad (1982) during measurements in this preparation with extracellular potassium-sensitive microelectrodes. Low calcium Ringer's solution has been routinely used in frog ventricular tension (Morad and Orkand, 1971) and membrane potential (Niedergerke and Orkand, 1966) studies. This preparation will continue to display normal electrical and mechanical responses for many hours in low calcium Ringer's solution, although the twitch tension is considerably reduced. However, additional experiments were performed at higher bath $[Ca^{++}]$ levels (0.5 and 1.0 mM) where similar percent depletions were seen for slow rates (1 to 24 per minute). The electrode was dislodged for faster rates in these higher calcium solutions.

In all frog hearts tested with extracellular single-barrel Ca-ISEs (n = 70), we found that acute increases in heart rate were associated with significant $[Ca^{++}]_o$ depletions (representative data shown below in Fig. 5). In ~25% of these preparations, an extracellular impalement was stable for more than 1 h, allowing us to perform an assortment of reproducible protocols. Before this, we had reported (Dresdner et al., 1982) results from experiments using double-barrel calcium ion-selective microelectrodes (n = 30 frog hearts). The double-barrel Ca-ISE electrodes were constructed and used as previously described for potassium ISEs (see Kline and Kupersmith, 1982; and Kline and Morad, 1978). Double-barrel Ca-ISEs were useful in measuring calcium depletions in the small cleft spaces where extracellular electrical potential fluctuations (V_o) were also seen during single beats. The second barrel of the double-barrel Ca-ISE measured these local electrical potentials and allowed for their subtraction from the Ca^{++}-induced potentials on the Ca^{++}-ion-selective barrel (Fig. 3; see also description by Kline and Morad, 1978 for K-ISEs).

We were able to measure beat-to-beat depletions in these cleft spaces with double-barrel Ca-ISEs (see Dresdner et al., 1982). However, the reduced response time of the Ca-ISE relative to the K-ISE and the difficulties encountered in trying to determine the exact location of the electrode tip in the small cleft spaces lead us to temporarily abandon the double-barrel electrode as a tool for developing a quantitative estimate of the transmembrane Ca^{++} flux.

However, we did make several qualitative observations. (*a*) For tip positions where extracellular potential fluctuations were visible, the beat-to-beat calcium depletions were large (averaging 10 to 25% of bath $[Ca^{++}]$; see Fig. 3) and had rapid components with one or two time constants (both <5 s). (*b*) For tip positions where no extracellular potential fluctuations where seen (i.e., no V_o), the beat-to-beat depletions were smaller and had a single slow time constant (20–120 s) comparable with that of the slow baseline depletion seen as the summation of the beat-to-beat changes. In case *a* the depletion reached a maximum simultaneously with the action potential repolarization; whereas, for case *b* the beat-to-beat depletion reached a maximum following repolarization. We feel that case *a* represents a measurement in the subendothelial space and case *b* represents a measurement in the extratrabecular space (see Cohen and Kline, 1982; Fig. 8). (*c*) For some extracellular positions, neither beat-to-beat calcium depletions nor V_o offsets were observed.

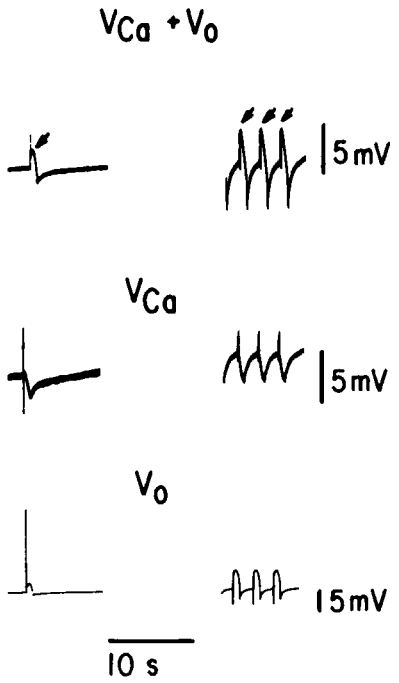

FIGURE 3 This figure shows double-barrel calcium-selective microelectrode responses at two different tip locations (*left* and *right* columns) in what we estimate to be the subendothelial space. The *right* column shows three beats in succession for a fiber equilibrated at a fast stimulation rate. The *left* column shows a single beat. The extracellular potential (V_o trace) shows characteristic miniature action potentials during beats. A detailed cable analysis would show that ~5% of the resistance drop between the intracellular space and the bath is distributed across the endothelial trabecular sheath (Dresdner, K., and R. P. Kline, unpublished calculation). This resistance drop across the sheath is likely responsible for the transient V_o change. Baseline shifts in V_o, if seen at all for such double-barrel Ca-ISE tip positions, were quite small and were always $\lesssim$20% of the more transient V_o deflection. The *top* trace ($V_{Ca} + V_o$) shows the output of the calcium-selective barrel. The output is biphasic and has an initial positive response due to the extracellular potential (V_o; see solid arrows). The subsequent negative going component is the calcium depletion response, which is shown (after compensation for V_o) in the differential output (*middle* trace). Each millivolt indicates 8% depletion of the calcium level (bath is 0.2 mM Ca^{++}). Thus the calcium-selective barrel alone (and hence a single-barrel Ca-ISE) can detect the presence of V_o changes; but the differential recording is required to compensate for the V_o changes.

Fig. 4 shows records for such a Ca-ISE extracellular tip position. Case *c* most likely represents measurements in the largest extratrabecular spaces. Thus we feel justified in using single-barrel Ca-ISEs to measure the slow component of the depletion in extracellular locations where there is no measurable V_o change and only minimal, if any, beat-to-beat depletion (see also Kline and Morad, 1978).

The V_o trace could easily be seen on the single-barrel electrode as a transient positive deflection occurring simultaneously with the action potential upstroke (see Fig. 3). The characteristic biphasic response of the V_o positive going trace, followed by a slower more sustained negative deflection (beat-to-beat calcium depletion response) clearly indicated that the single-barrel Ca-ISE tip was in a small cleft and should be repositioned. We found no evidence from the double-barrel Ca-ISE experiments of a baseline V_o shift that was more than a minor portion (~20%) of the transient V_o change. We could detect the transient V_o change; and by avoiding it, also avoided the possibility of a baseline V_o shift.

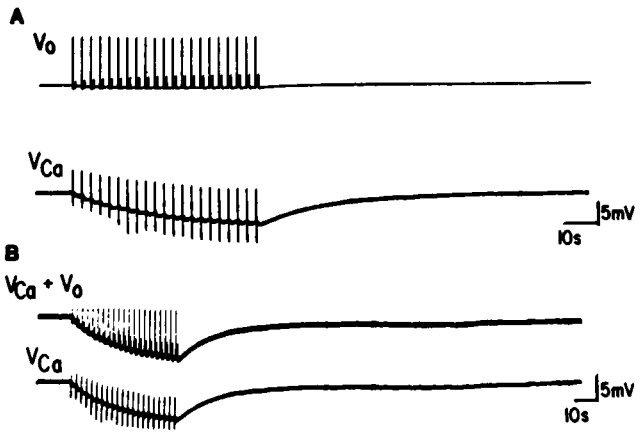

FIGURE 4 This figure shows the response of a double-barrel calcium-ion selective microelectrode during a short train (50 s) of repetitive stimulation at 24 beats per minute. The microelectrode tip is in an extracellular position where there is no baseline or cycle-dependent change in the extracellular potential (V_o; i.e., reference barrel output). In *A* (*top* trace), V_o shows only rapid transient deflections due to the stimulus artifact. These do not sum or alter the baseline. The *bottom* trace (V_{Ca}; the differential output of the two barrels) shows a slow negative going baseline deflection, which returns to original levels following cessation of stimulation. The V_{Ca} trace indicates a 50% reduction in original extracellular calcium levels of 0.2 mM. In *B*, we compare the calcium barrel alone ($V_{Ca} + V_o$; *top* trace) with the differential output (V_{Ca}; *bottom* trace). The *top* trace is what is recorded by a single barrel Ca-ISE. Note the slower chart speed in *B*. The depletions indicated by the *top* and *bottom* traces are nearly identical, as expected, since the baseline V_o changes were negligible.

The use of single-barrel Ca-ISEs greatly simplified our experiments, since these electrodes (*a*) were easier to construct (*b*) had smaller tip sizes causing less tissue damage, and (*c*) were more reliably constructed due to the more effective silanizing techniques applicable to single-barrel but not double-barrel electrodes.

To measure the $[Ca^{++}]$ in the extratrabecular space of a frog ventricular strip, a Ca-ISE was slowly inserted into the myocardium under constant observation through a dissecting microscope to prevent dimpling the tissue. Sometimes cells were punctured while the Ca-ISE was being advanced into the tissue. However, slight withdrawal or further advances of the microelectrode's tip returned the Ca-ISE potential to that observed in the bath Ringer's solution, and made it responsive to later changes in the bath $[Ca^{++}]$. The size of the extratrabecular spaces (where we believe the Ca-ISE tips were lodged) are on average 5 to 10 μM in width. The size of the spaces under the trabecular sheaths (subendothelial space) average 5 μM in width. Both space can readily accomodate the Ca-ISE tips.

RESULTS

Fig. 5 *a* (lower trace) is a representative experimental record of the change in the extracellular $[Ca^{++}]$ that occurs during an acute increase in heart rate. The ventricular action potentials accompanying this result are shown in the upper trace. The decrease in the diastolic membrane potential probably is due to extracellular $[K^+]$ accumulation (Kline and Morad, 1976, 1978). When the prior stimulation rate was resumed, the change in the $[Ca^{++}]_o$ and in the diastolic membrane potential reversed slowly back to predrive levels.

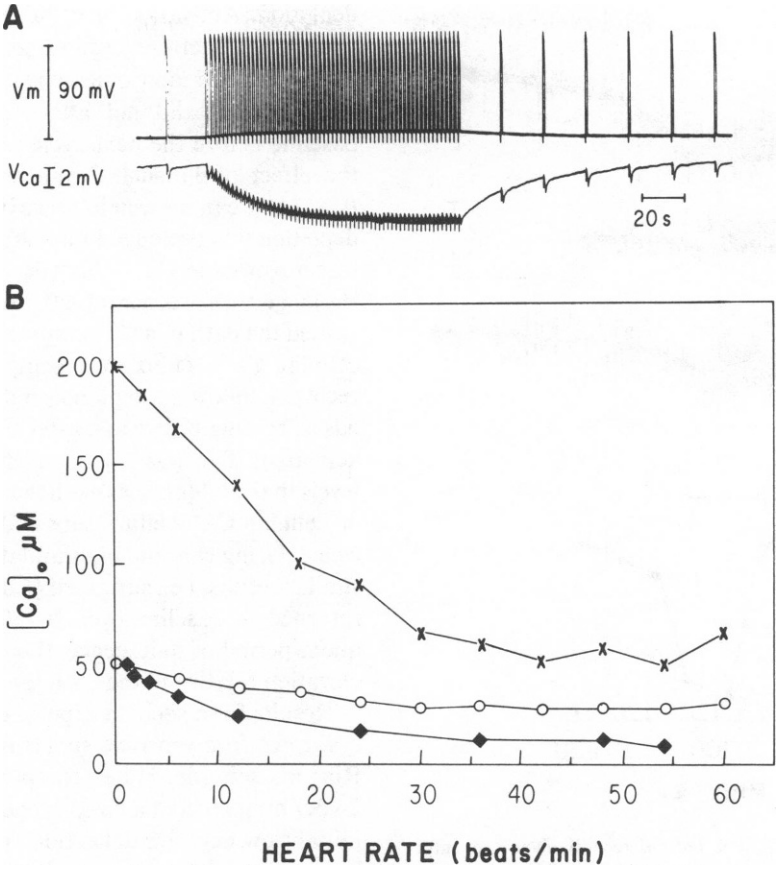

FIGURE 5 In *A*, the *top* record is the membrane potential (V_m) measured simultaneously with the output ($V_{Ca^{++}}$) of a single-barrel calcium ion-selective microelectrode (*bottom* record). As the heart rate is acutely increased from 3 to 30 per minute for 2 min, $[Ca^{++}]_o$ falls from 50 to 30 μM. Small beat-to-beat $[Ca^{++}]_o$ depletions are sometimes seen. The rapid vertical spikes in all $V_{Ca^{++}}$ records are stimulus artifacts. In *B*, we plot the $[Ca^{++}]_o$ level (vertical axis) at the end of 2 min of stimulation as a function of heart rate (horizontal axis). The superfusate Ringer's solution $[Ca^{++}]$ and calcium microelectrode tip depth were varied. Note the graph symbols. X is 200 μM $[Ca^{++}]$ and 0.6 mm depth. O is 50 μM $[Ca^{++}]$ and 0.3 mm depth. ♦ is 50 μM $[Ca^{++}]$ and 0.6 mm depth. The length of the neutral Ca^{++} carrier resin column was measured under a microscope after the electrode was constructed. By then observing the length of the resin column visible (using a calibrated eyepiece), after the electrode was inserted into the myocardium, one could estimate the depth of the microelectrode in the strip. Each point is the mean of two trials.

Fig. 5 *b* plots the dependence of the final $[Ca^{++}]_o$ level upon the acute heart rate. The absolute magnitude of $[Ca^{++}]_o$ depletion (attained after 2 min of repetitive field stimulation) increased as the acute heart rate was increased from 1 to 48 per minute. $[Ca^{++}]_o$ depletion occurred at rates >1 per minute, a lower acute rate threshold than for $[K^+]_o$ accumulation (Kline and Morad, 1978). The absolute magnitude of the $[Ca^{++}]_o$ depletion was approximately four times larger in 0.20 vs. 0.05 mM $[Ca^{++}]$ Ringer's solution. The depletion was smaller at shallower radial depths. The maximal $[Ca^{++}]_o$ depletion in ~1 mm wide ventricular strips was attained 3–5 min following an acute increase in heart rate. In one preparation superfused with 1.0 mM $[Ca^{++}]$ Ringer's solution, depletions of ~300 μM occurred after 2 min of field stimulation at 12 per minute. Stable tip positions were maintained for only brief trains at low heart rates in this higher $[Ca^{++}]$ Ringer's solution. The time constants of the depletions and the final levels of depletion obtained at low stimulus rates were used to estimate the net transmembrane Ca^{++} flux associated with each cardiac cycle. Such results are described in the analysis section.

Fig. 6 *a* shows the effect of manganese ion (1.0 mM in 0.20 mM $[Ca^{++}]$ Ringer's solution) on cumulative $[Ca^{++}]_o$ depletion caused by an acute increase in the heart rate. Since manganese ions have been shown to block the slow inward current carried by Na^+ and Ca^{++} ions (Rougier et al., 1969), reduce twitch tension (Chapman and Ellis, 1977), and are thought to inhibit Na^+/Ca^{++} exchange (Baker, 1972), then the cumulative $[Ca^{++}]_o$ depletion should be reduced by extracellular manganese ion. Manganese ion reversibly blocked the magnitude of the $[Ca^{++}]_o$ depletion by 56 ± 9% ($n = 5$) while only shortening the action potential duration by 14 ± 2% ($n = 4$). The time course of the effect of manganese ions upon the magnitude of the $[Ca^{++}]_o$ depletion was plotted in Fig. 6 *b*. This plot shows that the effect of manganese was reversible.

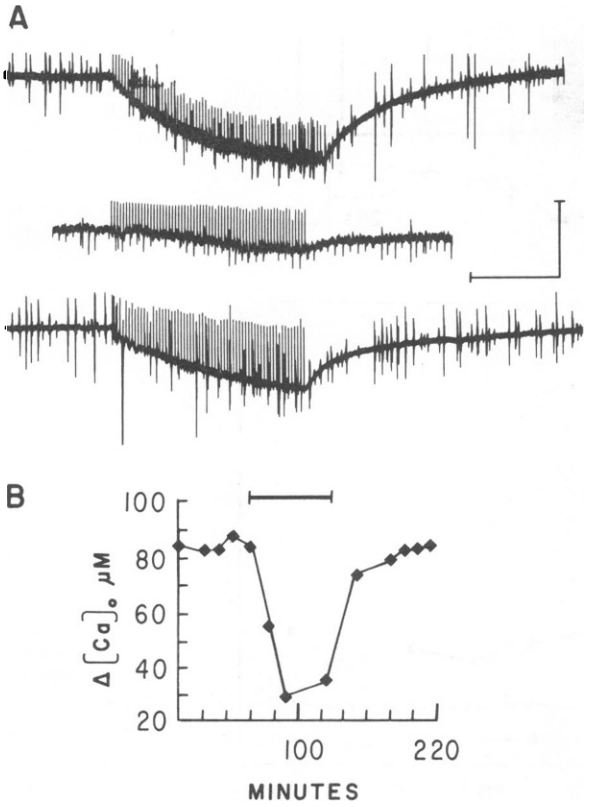

FIGURE 6 In *A*, *top*, *middle*, and *bottom* records show the output ($V_{Ca^{++}}$) of the single-barrel calcium ion-selective microelectrode during repetitive stimulation at 30 per minute for 2 min following a period of quiescence. The *top* and *bottom* traces (pre- and post-controls) show the $[Ca^{++}]_o$ depletion in 0.20 mM $[Ca^{++}]$ Ringer's solution. The *middle* trace shows the effect of addition of 1 mM manganese ion to the Ringer's solution. The irregular spikes are bath drainage artifacts. The bracket's vertical value is 5 mV and horizontal value is 1 min. In *B* the *bottom* panel plots the magnitude of the $[Ca^{++}]_o$ depletions (vertical axis) at the end of 2 min trains at 30 per minute. Each solid diamond represents the value for the magnitude of the $[Ca^{++}]_o$ depletion of a single train. Manganese ion (1 mM) was added for times (horizontal axis) as shown with the black horizontal bar (times between 60 and 130 min). This concentration of Mn^{++} did not influence the calcium microelectrode response to a 10 μM $[Ca^{++}]$ calibrating solution by more than 1 mV. This indicates that the electrode selectivity for Ca^{++} over Mn^{++} was >1,000:1. Thus the 1 mM Mn^{++} appeared to the Ca-ISE as 1 μM Ca^{++} and generated an 0.5% error in the 0.2 mM Ca^{++} Ringer's solution.

The capacity of frog ventricular cells to store Ca^{++} must be finite. Therefore at steady state the net transmembrane Ca^{++} flux per cardiac cycle (systole plus diastole) should be zero. Since $[Ca^{++}]_o$ depletion can persist for many minutes when the heart rate is suddenly increased, we designed a protocol to study the frog ventricular cell Ca^{++} extrusion mechanism. We found (Dresdner et al., 1982) that it had a slower rate of activation than the Na^+/K^+ATPase pump in this preparation (Martin and Morad, 1982).

Fig. 7 shows the results of an experiment designed to examine the effect of cellular Ca^{++} extrusion on $[Ca^{++}]_o$ depletion. Activation of cellular Ca^{++} efflux was accomplished by repetitive cycling between a 1-min stimulation period and a 1-min quiescence period (Fig. 7 *a* records). This protocol did not allow the $[Ca^{++}]_o$ to return to baseline before the next cycle was initiated. Fig. 7 *b* plots the effect of 11 such 2-min cycles on the extracellular $[Ca^{++}]$. It can be seen in this experiment that the $[Ca^{++}]_o$ depletion was prolonged for ~20 min at which time the net transmembrane Ca^{++} flux (per 2 minute cycle) was zero. Prolonged quiescence at 20 min caused the $[Ca^{++}]_o$ to exceed the bath $[Ca^{++}]$ presumably as a result of enhanced cellular Ca^{++} efflux. We compared the rate of $[Ca^{++}]_o$ recovery following depletion induced by one minute periods of beating before and after Ca^{++} efflux was apparently activated. The $[Ca^{++}]_o$ recovered more rapidly to bath levels in the later cycles as shown in Fig. 7 *c*. The activation of cellular Ca^{++} efflux subsided during prolonged quiescence. Using continuous stimulation protocols we obtained similar results, i.e., sustained $[Ca^{++}]_o$ depletion only slowly returned to baseline over 20–30 min. During the subsequent period of quiescence, there was a transient $[Ca^{++}]_o$ elevation relative to the bath level lasting 20–30 min.

Results from such an experiment are shown in Fig. 8 for a strip of frog ventricle superfused with 0.5 mM $[Ca^{++}]$ Ringer's solution. When the preparation is stimulated at 24 per minute from a basal rate of 6 per minute, there is an initial slow negative deflection on the Ca-ISE output (Fig. 8, trace *A*). The electrode response is quantitatively similar to the responses seen in experiments with 10 times lower bath calcium (see Fig. 5 *a*). Since the Ca-ISE output is essentially proportional to the logarithm of the free extracellular calcium ion concentration, the similarity of the electrode's potential deflections at these two bath calcium levels (50 μM and 0.5 mM) indicates that the percent depletions are similar. The more detailed analysis presented below will show the strong dependence of the Ca^{++} influx per beat on the bath $[Ca^{++}]$.

When stimulation is continued beyond several minutes, the measured $[Ca^{++}]_o$ level slowly rises up towards the baseline $[Ca^{++}]$ (0.5 mM, Fig. 8, trace *A*). Upon cessation of stimulation (Fig. 8, trace *B*), $[Ca^{++}]_o$ overshoots the baseline for tens of minutes. These data are plotted as the extracellular calcium concentration vs. time (Fig. 8, graph). Kunze (1977), Martin and Morad (1982), and Kline and Kupersmith (1982) attributed the poststimulation $[K^+]_o$ depletion to an enhanced level of activity of the transmembrane sodium-potassium ATPase pump. We suggest the $[Ca^{++}]_o$ overshoot occurs when the net transmembrane Ca^{++} flux is outward and attribute the net outward Ca^{++} flux to the enhanced activity of a transmembrane Ca^{++} transport mechanism(s). This mechanism undoubtedly activates in response to the amount of Ca^{++} accumulated inside the frog ventricular cells during the period of prolonged repetitive depolarizations. We have termed this mechanism a "Ca^{++} extrusion process" here

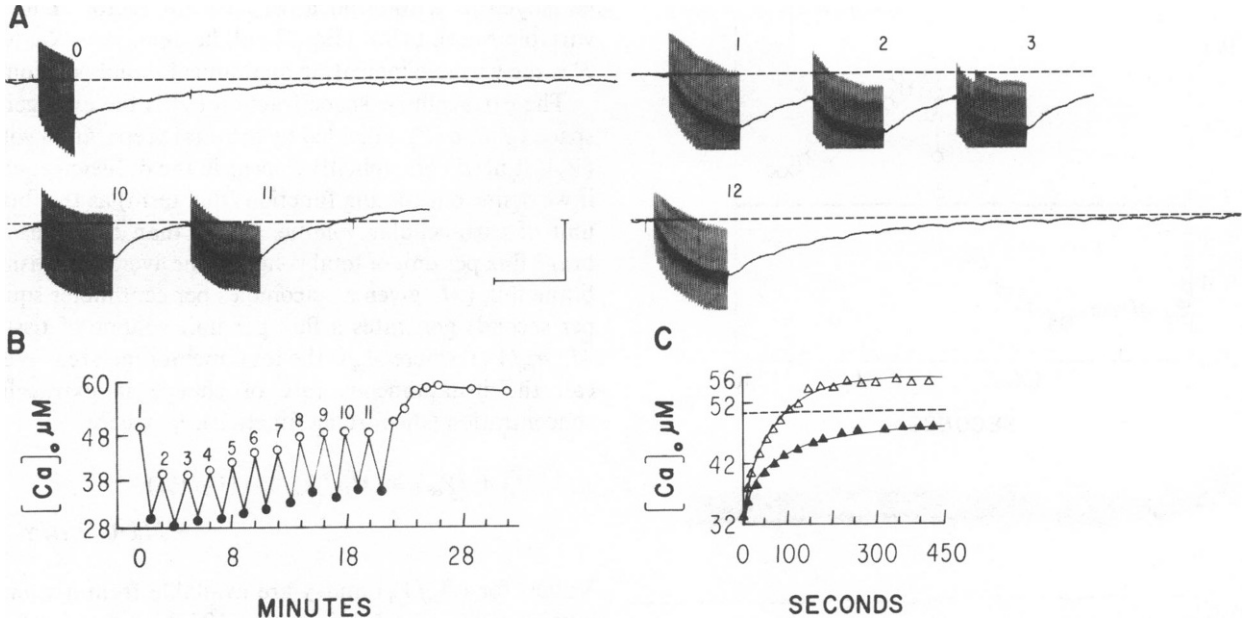

FIGURE 7 In *A*, records of the output of a single-barrel calcium ion-selective microelectrode are shown and depletions (stimulation cycles) are numbered to correspond to the numbering in the graph (*B*). The dashed line indicates the value corresponding to bath $[Ca^{++}]$ (50 μM). Each stimulus cycle consists of 1 min at a heart rate of 48 per minute followed by 1 min of quiescence. Cycle *0* is a short control stimulus train (duration 30 s) before the application of 11 consecutive cycles (numbered on the figure as *1* through *11*). Cycle *12* is a 1-min stimulus train 30 min after termination of cycle *11*. Note that there is a net depletion following the first two cycles (*1* and *2*), but there is no net depletion following *10* and *11* by which time we hypothesize that a Ca^{++} extrusion process is activated. Consistent with this hypothesis is the observation that there is an accumulation of $[Ca^{++}]_o$ during the prolonged quiescence after *11*. Note also, that the depletions during *1* and *12* are similar in magnitude and both are larger than *11* even though all three cycles started at the same (bath) $[Ca^{++}]_o$ levels. The depletion during *11* is equal in magnitude to that during *0* even though *0* is half the duration of *11* and both started from the same bath $[Ca^{++}]_o$ levels. (The calibration bars indicate 5 mV and 1 min for the vertical and horizontal bars, respectively). The plot in *B* shows $[Ca^{++}]_o$ levels vs. time for cycles 1–11. ○ marks the $[Ca^{++}]_o$ just before the 1-min stimulation period and ● marks the $[Ca^{++}]_o$ at the end of the 1-min stimulation period. The reduction in the magnitude of the depletion from cycle *1* to cycle *2* is most likely not due to the Ca^{++} extrusion mechanism that activates much more slowly, but rather due to the reduced ambient $[Ca^{++}]_o$ levels and the diffusion properties of the extracellular space. That a reduced ambient $[Ca^{++}]_o$ level reduces the absolute $[Ca^{++}]_o$ depletion (i.e., reduces net cellular Ca^{++} influx) is consistent with Fig. 5 *b*. Furthermore, a diffusion analysis would indicate that the larger the bath to extracellular space $[Ca^{++}]_o$ gradient, the more rapidly that Ca^{++} diffuses into the extracellular space surrounding the Ca-ISE tip from the bath to counter the effects of the influx of Ca^{++} into the cells. This is consistent with the observation that from cycles *2* to *11* the depletions get larger as the level of the $[Ca^{++}]_o$ envelope increases, approaching the bath $[Ca^{++}]$. *C* plots and compares the off tails following cycles *0* and *11*. Both depletions start at the same bath $[Ca^{++}]$ level and end at 33 μM. Since the Ca^{++} extrusion process is active in cycle *11*; its depletion is equal to that of cycle *0*, which is a shorter train. The recovery (off) tail of cycle *11* (△) is more rapid than the recovery tail of cycle *0* (▲). The tail of cycle *11* overshoots the bath $[Ca^{++}]$, indicative of net cellular Ca^{++} efflux. Note this is also shown in the final quiescence period in *B*.

since we did not attempt to determine whether the Ca^{++} efflux was via Na/Ca exchange or a Ca^{++}-ATPase or both.

The large time constant for activation of this Ca^{++} extrusion process (8–10 min) eliminated an important complication in estimating the net transmembrane flux of calcium during rapid beating. There was negligible activation of this calcium transport system following stimulus trains of <4 min, as evidenced by the consistent lack of a detectable postdrive $[Ca^{++}]_o$ overshoot. In the analysis section below we used 2–4-min trains of stimulation to evoke $[Ca^{++}]_o$ depletion from which we estimated the net transmembrane calcium flux. Thus we have assumed that this Ca^{++} extrusion process does not play a role in reducing the net transmembrane Ca^{++} influx during short, rapid stimulus trains. It is important to point out that there is no evidence that the long time constant for activation of the calcium extrusion mechanisms is due to a delayed response of the Ca^{++} transporter to elevated intracellular calcium activity. Rather, it is more likely that the time constant represents the time required to saturate the intracellular buffering capacity of the cell, and that the transporter is continuously responding to the slowly increasing levels of intracellular calcium activity.

Analysis

The assumptions underlying the quantitative estimates developed in this section are described in detail in treatments by Nicholson (1980), Cohen and Kline (1982), and Kline and Kupersmith (1982; Appendix). They will be

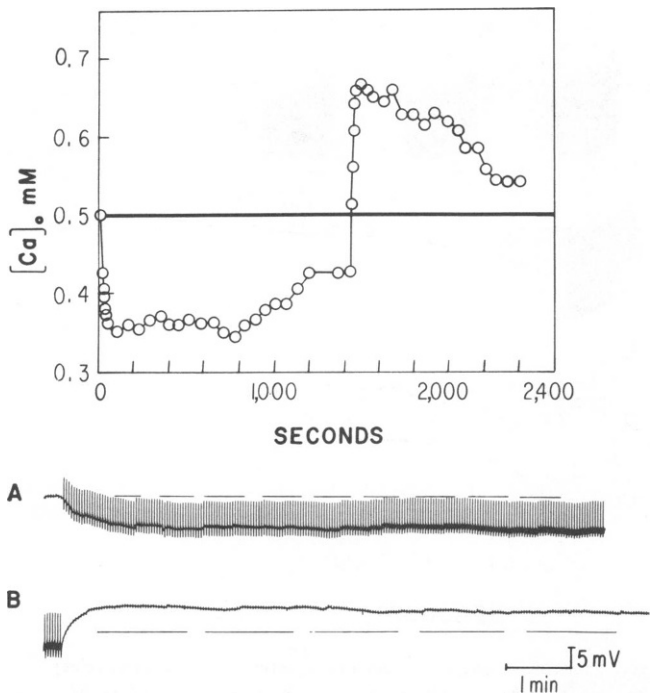

FIGURE 8 *Top* plot was digitized from records shown below in *A* and *B*. The plot shows that when the rate of repetitive stimulation is increased suddenly from 6 to 24 per minute for a frog ventricular strip bathed in 0.5 mM [Ca^{++}], the extracellular free calcium ion concentration falls by ~30% (from 0.5 to 0.35 mM) in 2 min. With continued stimulation the depletion is maintained near that level for approximately the next 10 min indicating sustained net cellular Ca^{++} uptake by the preparation. The bath level is indicated by the dashed line in the actual experimental records (*A* and *B*) and by a solid line in the plot on *top*. The $[Ca^{++}]_o$ level slowly increased during the later part of the stimulation (24 per minute) to 0.44 mM. After 20 min, the stimulation rate was then returned to 6 per minute. At this time $[Ca^{++}]_o$ rapidly increased from 0.44 to 0.67 mM within 1 min. It then slowly decreased over the next 15 min to 0.54 mM when the experiment was terminated. Calibration bars indicate 1 min time (horizontal) and 5 mV Ca-ISE response (vertical) for *A* (response to high stimulus rate) and *B* (return to low stimulus rate).

briefly reiterated at this time. Kline and Kupersmith (1982) used the diffusion equation (in appropriate coordinates) to generate analytical solutions of ion diffusion. Net transmembrane flux is represented as a forcing function added to the diffusion equation. Although this forcing function can have explicit dependence on time (Kline and Kupersmith, 1982, Eq. 4) or local concentration of the diffusing ion (Nicholson, 1980, Eq. 6), we assume in this treatment that it is a constant.

The diffusion equation is most directly applied for free diffusion. The presence of cardiac cells and connective tissue sheaths provide inhomogeneous obstructions to free diffusion in our tissue preparation. However, this difficulty can be handled if two additional distributed anatomical parameters are introduced (Nicholson, 1980): (*a*) the tortuosity constant (λ); and (*b*) the extracellular space fraction (γ). The tortuosity constant (λ) incorporates the average lengthening of diffusion distances due to the requirement of diffusion around obstructions. It is employed as a multiplicative constant factor. Thus, the variable r used below (Eq. 2) will be defined as $R\lambda$, where R is the variable indicating anatomical radial position.

The extracellular space fraction (γ) is the extracellular space volume (V_{ecs}) divided by the total preparation volume (V_T). It need not explicitly appear in the diffusion equation if we define our forcing function (flux term) as the flux per unit of extracellular volume, rather than the transmembrane flux per unit of total volume. The average transmembrane flux ($\overline{M}_j$; given as picomoles per centimeter squared per second) generates a flux per unit volume of tissue of $\overline{M}_j(A_m/V_T)$, where A_m is the total membrane area. We will call the instantaneous rate of change in extracellular concentration (the forcing function), j_{Ca} where

$$j_{Ca} = \overline{M}_j(A_m/V_{ecs}) = (\overline{M}_j)\,(A_m/V_T)\,(V_T/V_{ecs}) = \overline{M}_j(A_m/V_T)/\gamma\,. \quad (1)$$

Values for (A_m/V_T) and γ are available from anatomical studies (Page and Niedergerke, 1972), and are taken as 0.75 μ^{-1} and 0.25, respectively. Thus we can solve for j_{Ca} and later convert this value to M_j or the transmembrane net calcium current. Using simple geometric relations, the change in total intracellular calcium per second ($d[Ca]_i/dt$) can also be calculated from the ratio of intracellular to extracellular space volumes ($V_{ics}/V_{ecs} = 3$) and from j_{Ca} to be $j_{Ca}/3$. If we let the extracellular calcium concentration ($[Ca^{++}]_o$) be denoted as $Ca_o(r, t)$, a variable that is a function of radius and time, the appropriate equation in cylindrical coordinates is now

$$\partial\, Ca_o(r,t)/\partial t = D_{Ca}\,\{\partial^2/\partial r^2 + [(1/r)\,(\partial/\partial r)]\}\, Ca_o(r,t) + j_{Ca}\,. \quad (2)$$

We use cylindrical coordinates for simplicity and as the best approximation of the shape of the preparation. Since the measured time constant of the depletion is required to perform the final approximation rather than an estimate of the actual dimensions (see Eq. 6), the error due to the preparation deviating from the chosen simple geometric shape is minimized. (See Appendix.)

The value of j_{Ca} that we will calculate is the average rate of influx over the entire cardiac cycle. If we assume that most of the flux occurs during the action potential for short stimulus trains where there is no pump efflux, then the rate of flux during the action potential is obtained by multiplying j_{Ca} by the stimulus interval (SI) and dividing by the action potential duration (APD).

We use slow rates of stimulation (3–18 per minute) for these protocols for several reasons. During each beat, the calcium fluxes are likely to generate gradients of $[Ca^{++}]_o$ within the narrow clefts between cells and across the endothelial sheath (Cohen and Kline, 1982; Kline and Morad, 1978). At slow stimulus rates, these gradients are given more time to decay such that these restricted spaces can equilibrate with the larger extracellular spaces before

the next beat. This allows us to neglect the extracellular ionic inhomogeneity associated with the small clefts and concentrate on the large radial gradients that develop slowly during the stimulus train.

Secondly, by using slow stimulus rates, the radial gradients are small enough such that we can neglect implicit radial dependence of the average rate of influx. For example, a reduction of $[Ca^{++}]_o$ at the center of the preparation to 50% of the bath level would certainly reduce the rate of calcium transmembrane flux for cells at the center of the preparation. At the same time, the superficial fibers would be exposed to normal bath calcium levels and have a normal transmembrane influx rate. The value of j_{Ca} would be radially dependent in this case. At high stimulus rates (24–60 beats per minute), there are marked and complex changes in the time course of depletion (Dresdner, K., and R. P. Kline, manuscript in preparation).

For the range of slow rates we used to generate data for the flux estimate, the following criteria were met: (*a*) the depletion could be fit by a single exponential (this clearly was not the case at higher rates); (*b*) the time constants of the falling phase of the depletion did not change significantly over the range of low rates and were comparable to the decay of the depletion (rising phase); (*c*) the time constants of the decay of depletion showed no systematic rate dependence; and (*d*) the slow stimulation rates were chosen from the range of rates over which there was a roughly linear dependence of the magnitude of the depletion on the rate (see Fig. 5 *b*, graph).

The time constants of both the falling and rising (post stimulus) phases of the depletions (20–100 s) were the values expected for diffusion of calcium in a cylindrical preparation of diffusion radius (*a*), where *a* varies between 304 and 680 μm (see Eq. 5; *a* is defined as λ times the anatomical radius).

Solutions to Eq. 2 are available (Kline and Kupersmith, 1982, Eqs. 4 and 5; Carslaw and Jaeger, 1959, Eq. 7.9.1). We will consider for our solution only the first term in the Bessel function expansion. This will generate no more than a 10% error for measurements at the center of the preparation ($r = 0$). This can be seen by comparing the value of the first term coefficient at r = 0 with the steady state solution at $r = 0$. This procedure is further justified by our ability to obtain good single exponential fits from the rising and falling phases of the calcium depletions seen at slow stimulation rates.

The total magnitude of the depletion (Δ $Ca_o[r]$) is then given by the coefficient for the first term in the Bessel expansion as follows:

$$\Delta Ca_o(r) = 2j_{Ca}[J_0(r\alpha_1)]/\{[J_1(a\alpha_1)](a\alpha_1)(D_{Ca}\alpha_1^2)\}. \quad (3)$$

This can be readily solved for j_{Ca} by algebraic manipulation

$$j_{Ca} = \Delta Ca_o(r)[J_1(a\alpha_1)](a\alpha_1)/\{(2\tau_1)[J_0(r\alpha_1)]\}, \quad (4)$$

where τ_1 is the time constant for this major component of the calcium depletion and is given by

$$\tau_1 = 1/(D_{Ca}\alpha_1^2). \quad (5)$$

From standard tables (Carslaw and Jaeger, 1959) we can obtain values for additional terms in this expression: $a\alpha_1 = 2.4048$; $J_1(a\alpha_1) = 0.516$; $J_0(0) = 1.0$. D_{Ca} equals 800 $\mu m^2/s$ in free solution (Wang, 1953).

Thus at the center of the preparation the value of j_{Ca} is readily obtained from the magnitude of the depletion $\Delta Ca_o(r = 0)$, and the time constant (τ_1) of the depletion, and is given by

$$j_{Ca} = \Delta Ca_o(r = 0)/(1.6\,\tau_1). \quad (6)$$

(One should avoid confusing j_{Ca}, the forcing function, with J_0 and J_1, the Bessel functions. The forcing function is equal to the instantaneous rate of depletion of calcium induced by the transmembrane net calcium influx at the start of the train. The Bessel function is a radial form factor that indicates the shape of the radial gradients.)

In Table I, we present values from a series of runs in three different bath calcium concentrations. We present values for magnitudes and time constants of depletion, and then calculate the average transmembrane flux (M_j) assuming that all the net transmembrane calcium movement occurs at a uniform rate and only during the action potential. Based on this assumption we must first multiply values of j_{Ca} by the ratio of the *SI* over the *APD*. This calculation gives us the flux values averaged over a single beat (M_j) rather than the flux value averaged over the stimulus interval ($\overline{M_j}$). The *APD* changed only minimally during a train of stimuli since slow stimulation rates were used.

Calculation of the net increase in intracellular calcium occurring during each beat is a useful value to assess whether activator calcium originates from the extracellular fluid during each beat. We can use our values for M_j to obtain the change in intracellular total calcium that occurs per beat. One can either multiply j_{Ca} from Eq. 6 by *SI* and the ratio of the extracellular to the intracellular spaces, i.e., $(j_{Ca})(SI)(V_{ecs}/V_{ics})$; or, one can multiply M_j by *APD* and the cell surface to volume ratio, i.e., $(M_j)(APD)(A_m/V_{ics})$. These two procedures are algebraically equivalent.

The values that we calculate for change in total intracellular calcium per beat in 0.05, 0.2, and 1.0 mM calcium Ringer's solution are, respectively, 0.48 ± 0.15, 1.3 ± 0.30, and 6.5 ± 1.4, in micromoles per liter of cells.

In a 1963 study of the frog heart (bathed in $^{45}Ca^{++}$-containing 1 mM Ca^{++} Ringer's solution) Niedergerke calculated the net transmembrane Ca^{++} influx per action potential to be 0.15 pmol/cm^2. In a later study of more careful design using $^{45}Ca^{++}$-containing 1.5 mM Ca^{++} Ringer's solution, the net influx per beat was determined to be 0.13 pmol/cm^2 (Niedergerke et al., 1969). In the present study, we calculate an average net transmembrane Ca^{++} influx of 0.81 ± 0.17 pmol/cm^2/s during an 800-ms

action potential for frog ventricular muscle superfused with 1 mM Ca^{++} Ringer's solution. This corresponds to a flux of 0.65 ± 0.14 pmol/cm^2 per 800-ms action potential and is four to five times larger than the above prior estimates. Tracer $^{45}Ca^{++}$ estimates of the net transmembrane Ca^{++} flux during beating of frog ventricle are thought to underestimate the flux (Niedergerke and Orkand, 1966; Niedergerke et al., 1976). Thus our higher estimates of the flux are more consistent with the hypothesis that contraction is induced in frog ventricle by Ca^{++} directly entering the cells during the action potential (Niedergerke et al., 1969).

TABLE I
ESTIMATED NET TRANSMEMBRANE Ca^{++} FLUX (M_j) AVERAGED OVER INDIVIDUAL BEATS FOR FROG VENTRICULAR MYOCARDIUM

Bath [Ca^{++}]	Heart rate	Depletion magnitude	Time constant (τ_1)	M_j during each beat; i.e., $(j_{Ca})(SI/APD)(V_{ecs}/A_m)$
mM/l	*beats/min*	*μmol/l* ECS		*pmol/cm²/s*
0.050	3	9	60	0.069
0.050	6	17	58	0.068
0.050	6	14	61	0.053
0.050	12	9	35	0.040*
0.050	18	10	31	0.033*
0.20	3	22	68	0.16
0.20	3	4	21	0.093‡
0.20	6	26	38	0.17‡
0.20	6	13	21	0.15
0.20	12	26	18	0.18‡
1.0	12	386	65	0.77
1.0	12	379	50	0.99
1.0	12	320	63	0.66

Data are presented from a series of experiments at three different levels of bath [Ca^{++}]. Bath [Ca^{++}] is shown in column 1 in millimoles per liter. Only heart rates of 18 per minute or below were used and are shown in column 2. Column 3 gives absolute depletion in micromoles of Ca^{++} per liter, measured at the end of the stimulus train (2–4 min). Column 4 gives time constants (τ_1) of this depletion as determined by a computerized exponential fitting subroutine (Prophet 52 time sharing facility; PDP 10 software developed by Bolt, Baranek, and Newman, Cambridge, MA; 'Expfit' subroutine in Prophet Public Procedures). The time constants of depletion in 1.0 mM Ca^{++} Ringer's solution were determined graphically. M_j was calculated from Eq. 6, which gave values of j_{Ca} (the instantaneous rate of change of extracellular calcium due to the calcium influx), and Eq. 1, which converted j_{Ca} into M_j. *APD* values were measured during the runs, but showed only minor variation during the stimulus trains (±5%). M_j for each run was calculated using the steady state *APD* of the stimulus train, which averaged 900, 850, and 800 ms at heart rates 3 to 24 per minute in 0.050, 0.20, and 1.0 mM [Ca^{++}] Ringer's solution. The asterisk (*) denotes two runs in which the Ca-ISE tip was not advanced all the way to the center of the preparation, but was estimated to be at $r = 0.5a$. The calculation required rederiving Eq. 6 from Eq. 4 using the new value of r in the term $J_0(r\alpha_1)$. The double dagger (‡) denotes three runs in which the entire ventricular wall was not used. Instead, a piece was dissected with noticeably smaller dimensions, as evidenced in the low value for τ_1. The average values of M_j plus or minus standard deviation with bath [Ca^{++}] 0.050, 0.20, and 1.0 mM were 0.053 ± 0.016 ($n = 5$); 0.15 ± 0.034 ($n = 5$); and 0.81 ± 0.17 ($n = 3$), respectively. As stated in the text, the values of M_j calculated in this table were made with the assumption that all of the net flux occurred uniformly and occurred only during the action potential plateau.

Recent experimental reports using frog myocardium based on the voltage clamp of single cells (Hume and Giles, 1983) and optical measurements of extracellular Ca^{++} depletion (Hilgemann and Langer, 1984*a*) also indicate that Ca^{++} influx during single beats maybe larger than previously thought. Hume and Giles (1983) estimated the net Ca^{++} influx during an action potential in single isolated bullfrog atrial cells by integrating the calcium currents measured during voltage clamp. They then calculated the net increase in total intracellular calcium. Since the surface area to volume ratio of the bullfrog atrial cells is within 20% of that of frog ventricular cells, we can directly compare their estimate of a 10 μmol calcium ion increase per liter of cell volume (2.5 mM bath calcium) to our estimate in frog ventricular cells of a 5.1 to 7.9 μmol increase (1.0 mM bath calcium). This is good agreement considering the shorter action potential duration in atrial vs. ventricular cells.

Hilgemann and Langer (1984*a*) optically measured extracellular calcium depletion in frog ventricle, and report depletions of total dye-accessible calcium of 2–4%. Our calculated values are 2.0 ± 0.4% in 1.0 and 0.2 mM bath calcium, and 2.9 ± 0.9% in 50 μM bath calcium. The quantitative agreement here between calcium ion selective electrodes and optical measurements are quite good.

DISCUSSION

There is significant and sustained depletion of the extratrabecular [Ca^{++}] in frog ventricular muscle during sudden increases in heart rate (Dresdner et al., 1982; Dresdner and Kline, 1983). The magnitude of the $[Ca^{++}]_o$ depletion increases for faster heart rates, for higher Ringer's solution [Ca^{++}], and for deeper radial depth. This rate and depth dependence was also observed for $[K^+]_o$ accumulation in this preparation (Kline and Morad, 1978). Manganese ion, which is known to reduce the slow inward current (Rougier et al., 1969) and believed to inhibit Na^+/Ca^{++} exchange (Baker, 1972), inhibits $[Ca^{++}]_o$ depletion (Dresdner and Kline, 1983), suggesting that the measurement of $[Ca^{++}]_o$ depletion is a reliable indicator of changes in net transmembrane Ca^{++} influx. Using standard solutions to the diffusion equation and $[Ca^{++}]_o$ depletion data we quantitatively estimated the net transmembrane Ca^{++} influx.

Previously reported $[K^+]_o$ accumulation in frog ventricle (Kline and Morad, 1978) has been shown to be correlated with diastolic membrane potential depolarization and possibly changes in action potential duration. However, the diastolic membrane potential and action potential duration are relatively insensitive to the changes in the $[Ca^{++}]_o$ measured here (Niedergerke and Orkand, 1966). On the other hand, frog ventricular twitch tension rapidly

responds to changes in the superfusate [Ca^{++}] (Kavaler et al., 1978). Brown and Orkand (1968) have studied the frog ventricular isometric twitch tension response to increased heart rates in the range of $[Ca^{++}]_o$ studied here. They found that the twitch tension staircase is negative (up to −60% in magnitude) for periods of 1 to 3 min at heart rates that do not shorten the action potential duration. We found that the rate threshold for the onset of cumulative $[Ca^{++}]_o$ depletion is surprisingly similar to that for the negative tension staircase, i.e., 1 beat per minute (Brown and Orkand, 1968). This initial negative tension staircase may be in fact a result of the $[Ca^{++}]_o$ depletions we have measured in this preparation.

After more than 3 min of repetitive stimulation in <1 mM [Ca^{++}] Ringer's solution the isometric twitch tension staircase becomes increasingly positive attaining steady state in 20–30 min or more. Niedergerke (1963) has attributed the positive tension staircase in frog ventricle to the loading of an intracellular compartment with Ca^{++}. Our results in Figs. 7 and 8 indicate that a cumulative $[Ca^{++}]_o$ depletion can persist during this time of higher heart rate. This sustained, cumulative $[Ca^{++}]_o$ depletion is indicative of a sustained net cellular uptake of Ca^{++}. It is reasonable to suggest that the cellular homeostasis of Ca^{++} in the frog ventricle (which determines the steady state twitch tension response) depends upon equilibrium of the transmembrane Ca^{++} fluxes.

Recently calcium-sensitive absorption dyes (antipyrylazo III and tetramethylmurexide) have been used to spectrophotometically monitor the mean extracellular [Ca^{++}] in mammalian cardiac muscle (Hilgemann et al., 1983; Hilgemann and Langer, 1984*b*) and in frog cardiac muscle (Hilgemann et al., 1984*a*; Cleeman and Morad, 1984). Our results are in agreement with these investigators using optical techniques. Substantial amounts of calcium ions leave the cardiac muscle extracellular spaces and accumulate in the cells during the cardiac action potential. During trains of action potentials extracellular Ca^{++} depletion is cummulative (Dresdner et al., 1982; Hilgemann et al., 1983). Following sudden increases in heart rate, repetitive stimulation allows increased cellular Ca^{++} uptake to exceed the level of Ca^{++} extrusion, resulting in net cellular Ca^{++} uptake.

The frog heart differs from the mammalian heart in the manner of the cellular Ca^{++} extrusion mechanism's kinetics. Hilgemann and Langer (1984) have found that Ca^{++} can be rapidly returned to the extracellular space during a single cardiac cycle in rabbit or by several cycles in rat, cat, and guinea pig ventricle, 2 to 30 s following a short train of beats causing cummulative extracellular depletion. We, and Hilgemann and Langer (1984*b*), tested for, but failed to find, such a sudden release of Ca^{++} in the frog heart. Another difference between the rabbit and frog heart is the time required for the mean extracellular Ca^{++} concentration to return to the bath level during prolonged stimulation. We have found that 20 to 30 min of continuous Ca^{++} depletion will occur when the frog heart is abruptly stimulated at faster heart rates. In contrast, in the rabbit heart the period of cummulative depletions lasts only 2 to 4 min. The cellular extrusion mechanisms respond more rapidly in the rabbit than in the frog heart.

The relaxation of frog heart contraction is widely held to require transmembrane extrusion of Ca^{++} during the period of relaxation, since sarcoplasmic reticular sequestration is thought to be insufficient (Fabiato and Fabiato, 1978; Chapman, 1979). In frog ventricle driven at low rates (6–18 beats per minute), we, and Hilgemann and Langer (1984*a*) have found that replenishment of extracellular Ca^{++} is only partially completed during muscle relaxation. Thus Ca^{++} accumulated by the cell during the action potential is not completely returned to the extracellular space during muscle relaxation, in contradiction to the model. At higher rates, Hilgemann and Langer (1984*a*) indicate that replenishment of extracellular Ca^{++} is virtually complete by the end of relaxation. We feel that this correlation between extracellular Ca^{++} replenishment and muscle relaxation at higher rates maybe fortuitous, resulting from the interaction of phasic influx of Ca^{++} each beat with the continuous slowly changing efflux of Ca^{++} that is dependent upon the integral of the net Ca^{++} flux over time. Therefore, relaxation does not necessarily depend on cellular efflux of activator calcium. We find no mechanism that extrudes the calcium influx associated with the action potential on a beat-by-beat basis.

The frog heart also differs from the mammalian heart in terms of the time course of Ca^{++} uptake during the action potential. In the mammalian heart, Bers (1983) finds that the extracellular Ca^{++} depletion occurs early in the cardiac action potential, declining before repolarization. In contrast, in the frog heart, the extracellular depletion occurs continuously during the action potential and only begins to decline as the action potential repolarizes (Dresdner et al., 1982, 1983; Cleeman and Morad, 1984).

Certain classical pharmacological interventions similarly affect the extracellular Ca^{++} depletions in mammalian and frog hearts. Catecholamines increase the magnitude of extracellular depletion occurring during single action potentials in guinea pig atria (Hilgemann et al., 1983) and in frog ventricle (Dresdner et al., 1983; Cleeman and Morad, 1984). Ca^{++} channel antagonists such as nifedipine (Hilgemann and Langer, 1984*b*) and cobalt ions (Bers, 1983) in mammalian heart and manganese ion in frog heart have been found to reduce extracellular calcium depletion.

Much more needs to be known before frog ventricular Ca^{++} uptake and extrusion can be accurately described with reference to various proposed mechanisms. Ca^{++} uptake may occur both by a slowly inactivating membrane channel (Rougier et al., 1969; Hume and Giles, 1983) or by sodium-calcium exchange (Chapman, 1979). Both of these mechanisms are voltage sensitive and could explain the known dependence of tension development upon depo-

larization of the membrane potential (Morad and Orkand, 1971). Possible Ca^{++} extrusion mechanisms include sodium-calcium exchange and Ca^{++}-ATPase (Caroni and Carafoli, 1981). Both of these mechanisms would respond to increases in cytoplasmic Ca^{++} activity. The high capacity of frog ventricular cells to buffer cytoplasmic calcium during cardiac activity (Niedergerke, 1963) may explain the long delay in activation of cellular Ca^{++} extrusion, which we have observed.

Further studies of changes in the extracellular calcium activity during beating in cardiac muscle using both optical techniques and calcium-sensitive microelectrodes should prove to be useful in studies of contractility and membrane Ca^{++} transport.

APPENDIX

The preparation is approximated as a cylinder in the analysis section. To the extent that the preparation deviates from this idealized form, there is a possibility of error in our estimates. We will assess the likely size of this error by examining the case of a preparation that is a large flat rectangular sheet of ventricular wall. Let the thickness (w) of the sheet be much smaller than either of the other two dimensions. We can then compare the $[Ca^{++}]_o$ depletions induced by identical fluxes (j_{Ca}) in such a ventricular sheet preparation ($w = 2a$) and in a long cylindrical preparation ($r = a$; assume the length of the cylindrical axis is much greater than the radius, a). Thus, we neglect edge effects in this treatment.

Using equations described in Carslaw and Jaeger (sections 3.14 and 7.9), one can determine that the magnitude of the $[Ca^{++}]_o$ depletion at the center of the sheet ($x = 0$; $-a \le x \le a$) would be twice that observed at the center of the cylinder ($r = 0$), if we considered the steady state (ss) terms in the diffusion equation solutions

$$\Delta Ca_o^{ss}(r) = -(j_{Ca}/D_{Ca})(a^2 - r^2)/4 \qquad (A1)$$

for the cylinder, and

$$\Delta Ca_o^{ss}(x) = -(j_{Ca}/D_{Ca})(a^2 - x^2)/2 \qquad (A2)$$

for the sheet. On the other hand, the time constant of the first term in the expansion for the sheet is 2.34 times greater than the analogous time constant for the cylinder. Thus, the time constant for the first expansion term of the diffusion equation solution for the sheet (τ_1^s) is

$$\tau_1^s = (4a^2)/(D_{Ca}\pi^2). \qquad (A3)$$

The ratio of τ_1^s to τ_1 (time constant for the cylinder; Eq. 5) is given by

$$\tau_1^s/\tau_1 = (4a^2/D_{Ca}\pi^2)(D_{Ca})(2.4048/a)^2 = (4/\pi^2)(2.4048)^2 = 2.34. \qquad (A4)$$

Thus for identical fluxes (j_{Ca}), both the depletion and the time constant are increased for the sheet vs. the cylindrical preparation. In fact, the value of the ratio of $[\Delta Ca_o^{ss}(r = x = 0)/\tau_1]$ for the sheet is ~15% less than that for the cylinder due to this error. This leads to an underestimate of the value of j_{Ca}. Applying the same derivation to the sheet as we did for the cylinder in Eq. 6, one can generate a better estimate for the sheet. Again, using only the first term in the expansion, we can estimate the depletion as

$$\Delta Ca_o(x = 0) = (j_{Ca}/D_{Ca})(a^2)(16/\pi^3)$$

and substituting from Eq. A3

$$= (4/\pi)(j_{Ca}\tau_1^s). \qquad (A5)$$

By algebraic manipulation, the analogous version of Eq. 6 for the sheet is then

$$j_{Ca} = \Delta Ca_o(x = 0)/(1.27\tau_1^s). \qquad (A6)$$

If one were to use Eqs. 6 or A6 in the analysis section without regard for determining whether the preparation was a cylinder or a sheet, the error involved would be at most 21% (neglecting the error involved in using only the first terms in the expansion of the solution). By assuming a cylinder in our analysis, we have probably slightly underestimated the Ca^{++} flux.

To the extent that the small depletions we measured at low rates could be assumed to generate a linearly dependent local reduction in calcium influx, the use of a constant j_{Ca} could no longer be justified. Thus the effects of such small depletions on the rate of influx might appear to be an additional source of error. However, modification of Eq. 2 to allow for a $[Ca^{++}]_o$ dependent component of j_{Ca} would not alter the validity of applying Eqs. 6 or A6. It can be readily shown (see section 15.7, Carslaw and Jaeger, 1959) that values of τ_1 and ΔCa_o would both be altered by the same amount, allowing the ratio of $(\Delta Ca_o/\tau_1)$ to be preserved.

Let j_{Ca} be changed to $j_{Ca}(1 + \beta\Delta Ca_o)$, the new $[Ca^{++}]_o$-dependent flux term (forcing function) in Eq. 2. The coefficient for the first Bessel term and its time constant will then both be altered by the multiplicative constant $1/[1 - (j_{Ca})\beta/D_{Ca}\alpha_1^2)]$. Since j_{Ca} is negative during depletions, this multiplicative constant will get smaller as j_{Ca} gets larger. As rate is slowly increased at low rates of stimulation, the value of j_{Ca} gets larger. Thus one might expect a slight decrease in τ_1 and $(\Delta Ca_o)(SI)$ as rate increases (i.e., as SI decreases). However, the ratio will remain unchanged. Note that the above analysis would also apply if the local $[Ca^{++}]_o$ depletion produced a linearly proportional change in the rate of release of Ca^{++} from an extracellular buffering source.

K. Dresdner was supported by GM-07163-06A1. R. P. Kline was supported by a Young Investigator Award and Program Project Grant (No. 30557) from the National Heart, Lung, and Blood Institute, an Irma Hirschl Career Scientist Award, and a Grant in Aide from the American Heart Association.

Received for publication 15 August 1983 and in final form 26 February 1985.

REFERENCES

Allen, D. G., and J. R. Blinks. 1978. Calcium transients in aequorin-injected frog cardiac muscle. *Nature (Lond.).* 273:509–513.

Attwell, D., D. Eisner, and I. Cohen. 1979. Voltage clamp and tracer flux data: Effects of a restricted extracellular space. *Q. Rev. Biophys.* 12(3):213–261.

Baker, P. F. 1972. Transport and metabolism of calcium ions in nerve. *Prog. Biophys. Mol. Biol.* 24:177–223.

Bers, D. M. 1983. Early transient depletion of extracellular Ca during individual cardiac muscle contractions. *Am. J. Physiol.* 244:H462–H468.

Brown, A. M., and R. K. Orkand. 1968. A down then up staircase in frog ventricle due to altered excitation contraction coupling. *J. Physiol. (Lond.).* 197:295–304.

Caroni, P., and E. Carafoli. 1981. The Ca^{++} pumping ATPase of heart sarcolemna: characterization, calmodulin dependence and partial purification. *J. Biol. Chem.* 256:3263–3270.

Carslaw, H. S. and J. C. Jaeger. 1959. Conduction of Heat in Solids. Clarendon Press, Oxford. Second ed. 424 pp.

Chapman, R. A., and D. Ellis. 1977. Effect of manganese ions on contraction of the frog's heart. *J. Physiol. (Lond.).* 272:331–354.

Chapman, R. A. 1979. Excitation contraction coupling in cardiac muscle. *Prog. Biophys. Mol. Biol.* 35:1–52.

Cleeman, L., and M. Morad. 1984. Optical measurements of extracellular calcium depletion in frog ventricular strips. *Biophys. J.* 45(2, Pt. 2):137*a*. (Abstr.)

Cohen, I., and R. P. Kline. 1982. K^+ fluctuations in the extracellular spaces of cardiac muscle: evidence from the voltage clamp and K+ selective extracellular microelectrodes. *Circ. Res.* 50:1–16.

Dagostino, M., and C. O. Lee. 1982. Neutral carrier Na^+- and Ca^{++}-selective microelectrodes for intracellular application. *Biophys. J.* 40:199–207.

Dresdner, K., R. P. Kline, and J. Kupersmith. 1982. Extracellular calcium ion depletion in frog ventricle. *Biophys. J.* 37(2, Pt. 2):239*a*. (Abstr.)

Dresdner, K., and R. P. Kline. 1983. Effects of epinephrine, Ni++, and Mn++ on extracellular Ca++ activity fluctuations in beating frog ventricle using calcium ion-selective microelectrodes. *Biophys. J.* 42(2, Pt. 2):75*a*. (Abstr.)

Fabiato, A., and F. Fabiato. 1978. Calcium induced calcium release of calcium from the sarcoplasmic reticulum of skinned cells from adult human, dog, cat, rat, and frog hearts, and from fetal and newborn rat ventricles. *Ann. NY Acad. Sci.* 307:491–521.

Hilgemann, D. W., M. J. Delay, and G. A. Langer. 1983. Activation-dependent cummulative depletions of extracellular free calcium in guinea pig atrium measured with antipyrylazo III and tetramethylmurexide. *Circ. Res.* 53:779–793.

Hilgemann, D. W., and G. A. Langer. 1984*a*. Extracellular calcium transients in frog ventricle measured with antipyrylazo III and tetramethylmurexide. *Fed. Proc.* 43(4):82D. (Abstr.)

Hilgemann, D. W., and G. A. Langer. 1984*b*. Transsarcolemmal calcium movements in arterially perfused rabbit right ventricle measured with extracellular calcium sensitive dyes. *Circ. Res.* 54:461–467.

Hume, J. R., and W. Giles. 1983. Ionic Currents in Single Isolated Bullfrog Atrial Cells. *J. Gen. Physiol.* 81:153–194.

Kavaler, F., T. W. Anderson, and V. J. Fisher. 1978. Sarcolemmal site of caffeine's inotropic action on the ventricular muscle of the frog. *Circ. Res.* 42(2):285–290.

Kline, R. P., and M. Morad. 1976. Potassium efflux and accumulation in heart muscle: evidence from K+ electrode experiments. *Biophys. J.* 16:367–372.

Kline, R. P., and M. Morad. 1978. Potassium efflux in heart muscle during activity: extracellular accumulation and its implications. *J. Physiol. (Lond.).* 132:537–558.

Kline, R. P., and J. Kupersmith. 1982. Effects of extracellular potassium accumulation and sodium pump activation on automatic canine purkinje fibers. *J. Physiol. (Lond.).* 324:507–533.

Kunze, D. L. 1977. Rate-dependent changes in extracellular potassium in rabbit atrium. *Circ. Res.* 41(1):122–127.

Lee, C. O., D. Y. Uhm, and K. Dresdner. 1980. Sodium-calcium exchange in rabbit heart muscle cells: direct measurement of sarcoplasmic Ca^{++} activity. *Science (Wash. DC).* 209:699–701.

Lee, C. O. 1981. Ionic activities in cardiac muscle cells and application of ion-selective microelectrodes. *Am. J. Physiol.* 241:H459–H478.

Martell, A. E., and R. M. Smith. 1974. *Critical Stability Constants.* Vol. 1: Amino Acids. Plenum Publishing Corp., New York. 269–272.

Martin, G., and M. Morad. 1982. Activity induced potassium accumulation and its uptake in frog ventricular muscle. *J. Physiol. (Lond.).* 328:205–227.

Morad, M., and R. K. Orkand. 1971. Excitation contraction coupling in frog ventricle: evidence from voltage clamp studies. *J. Physiol. (Lond.).* 219:167–189.

Mullins, L. J. 1977. A mechanism for Na/Ca transport. *J. Gen. Physiol.* 70:681–695.

Nicholson, C. 1980. Dynamics of the brain cell microenvironment. *Neurosci. Res. Prog. Bull.* 18(2):177–299.

Niedergerke, R. 1963. Movements of Ca in beating ventricles of the frog hearts. *J. Physiol. (Lond.).* 167:551–580.

Niedergerke, R., D. C. Ogden, and S. Page. 1976. Contractile activation and calcium movements in heart cells. *Symp. Soc. Exp. Biol.* 30:381–395.

Niedergerke, R., and R. K. Orkand. 1966. The dual effect of calcium on the action potential of the frog's heart. *J. Physiol. (Lond.).* 184:291–311.

Niedergerke, R., S. Page, and M. S. Talbot. 1969. Calcium fluxes in frog heart ventricles. *Pfluegers Arch. Eur. Physiol.* 306:357–360.

Oehme, M., M. Kessler, and W. Simon. 1976. Neutral carrier Ca^{++} microelectrode. *Chimia.* 30:204–206.

Page, S., and R. Niedergerke. 1972. Structures of physiological interest in the frog heart ventricle. *J. Cell Sci.* 11:179–203.

Rougier, O., D. Garnier, Y. M. Gargouil, and E. Coraboeuf. 1969. Existence and role of a slow inward current during the frog atrial action potential. *Pfluegers. Arch. Eur. Physiol.* 308:91–110.

Tsien, R. Y., and T. J. Rink. 1980. Neutral carrier ion selective microelectrodes for the measurement of intracellular free calcium. *Biochim. Biophys. Acta.* 599:623–638.

Wang, J. H. 1953. Tracer diffusion in liquids. IV. Self-diffusion of calcium ions and chloride solutions. *J. Am. Chem. Soc.* 75:1769–1770.